Hydrodynamics control shear-induced pattern formation in attractive suspensions

Zsigmond Varga, Vincent Grenard, Stefano Pecorario, Nicolas Taberlet, Vincent Dolique, Sébastien Manneville, Thibaut Divoux, Gareth Mckinley, James Swan

Hydrodynamics control shear-induced pattern formation in attractive suspensions

As Published: 10.1073/pnas.1901370116

Publisher: Proceedings of the National Academy of Sciences

Persistent URL: https://hdl.handle.net/1721.1/136210

Version: Final published version: final published article, as it appeared in a journal, conference proceedings, or other formally published context

Hydrodynamics control shear-induced pattern formation in attractive suspensions

Zsigmond Varga[a], Vincent Grenard[b], Stefano Pecorario[b], Nicolas Taberlet[b], Vincent Dolique[b], Sébastien Manneville[b], Thibaut Divoux[c,d], Gareth H. McKinley[e], and James W. Swan[a,1]

[a]Department of Chemical Engineering, Massachusetts Institute of Technology, Cambridge, MA 02139; [b]Laboratoire de Physique, École Normale Supérieure de Lyon, Université Claude Bernard, Université de Lyon, CNRS, F-69342 Lyon, France; [c]Centre de Recherche Paul Pascal, CNRS UMR 5031, 33600 Pessac, France; [d]MultiScale Material Science for Energy and Environment, Unité Mixte Internationale 3466, CNRS–Massachusetts Institute of Technology, Cambridge, MA 02139; and [e]Department of Mechanical Engineering, Massachusetts Institute of Technology, Cambridge, MA 02139

Edited by Steve Granick, Institute for Basic Science Center for Soft and Living Matter, Ulju-gun, Ulsan, South Korea, and approved May 13, 2019 (received for review January 24, 2019)

Dilute suspensions of repulsive particles exhibit a Newtonian response to flow that can be accurately predicted by the particle volume fraction and the viscosity of the suspending fluid. However, such a description fails when the particles are weakly attractive. In a simple shear flow, suspensions of attractive particles exhibit complex, anisotropic microstructures and flow instabilities that are poorly understood and plague industrial processes. One such phenomenon, the formation of log-rolling flocs, which is ubiquitously observed in suspensions of attractive particles that are sheared while confined between parallel plates, is an exemplar of this phenomenology. Combining experiments and discrete element simulations, we demonstrate that this shear-induced structuring is driven by hydrodynamic coupling between the flocs and the confining boundaries. Clusters of particles trigger the formation of viscous eddies that are spaced periodically and whose centers act as stable regions where particles aggregate to form flocs spanning the vorticity direction. Simulation results for the wavelength of the periodic pattern of stripes formed by the logs and for the log diameter are in quantitative agreement with experimental observations on both colloidal and noncolloidal suspensions. Numerical and experimental results are successfully combined by means of rescaling in terms of a Mason number that describes the strength of the shear flow relative to the rupture force between contacting particles in the flocs. The introduction of this dimensionless group leads to a universal stability diagram for the log-rolling structures and allows for application of shear-induced structuring as a tool for assembling and patterning suspensions of attractive particles.

attractive suspensions | pattern formation | hydrodynamic stability

Spherical particles suspended in a viscous fluid constitute a canonical system for rheological analysis and have played a key role in our fundamental understanding of multiphase flow (1). From the seminal work of Einstein on the viscosity of a dilute suspension of spheres (2, 3) to the recent progress in simulations of large numbers of particles interacting hydrodynamically (4), model suspensions have allowed physicists and engineers to attack complex problems such as energy storage in flow batteries and flow capacitors (5, 6), food texture and shelf life (7), or more recently collective dynamics in active matter (8, 9). The case of purely repulsive particles, e.g., hard-sphere–like particles, is now well understood at least up to packing fractions of 40% where the mechanics of frictional contacts between the particles do not play a significant role (10–13). Nonetheless, in most practical cases, suspended particles display weak attractive interactions, which result in the formation of clusters that can be disrupted by the stresses induced under flow. As a consequence, the overall behavior of a suspension of weakly attractive particles is dictated by a subtle competition between shear and attraction, which controls both cluster size and cluster shape (14). This competition yields a wealth of rheological behaviors, including wall slip (15), flow heterogeneities (16), and steady-state shear-banded flows (17) that are at the core of ongoing and intense scientific investigation (18, 19).

Here, we investigate a striking experimental observation reported ubiquitously in dilute suspensions of attractive particles with a wide variety of shapes and chemistries: When sheared in a confined geometry at low enough shear rate, attractive particles suspended in a Newtonian fluid tend to self-organize into log-rolling flocs aligned along the vorticity direction that result in a characteristic striped pattern (Fig. 1). Such a phenomenon, commonly referred to as shear-induced structuring, has been indirectly evidenced by light-scattering measurements and scanning electron microscopy and quantified by optical microscopy in a broad range of colloidal (sensitive to thermal fluctuations) and noncolloidal (insensitive to the same) systems, including colloid–polymer mixtures (20), attractive emulsions (21), and suspensions of carbon nanotubes (22) as well as carbon black (23, 24), alumina (25), microfibrillated cellulose (26), and graphene oxide (27) dispersions. To date, shear-induced log formation has been associated with the emergence of negative normal stresses (21, 23), suggesting that vorticity alignment could be the consequence of an elastic instability occurring locally within

Significance

Flows of particulate suspensions are ubiquitous in advanced technological applications, including coating of colloidal inks and paints, manufacturing of pharmaceuticals, and oil production. When particles aggregate due to attractive forces, flow can induce giant anisotropic concentration fluctuations. Surprisingly, shear flow between parallel plates organizes these fluctuations into periodically spaced, particle-rich stripes that are aligned perpendicularly to the flow direction. We use experiments and complementary simulations to build a universal stability criterion, demonstrating that hydrodynamic interactions alone drive this process of pattern formation independent of particle size, shape, and chemical composition. Such flow-induced patterning has potential applications in the production of a broad range of anisotropic structures for use in technologies such as flexible electronics and nanocomposites, 3D printing, and flow batteries.

Author contributions: N.T., S.M., T.D., G.H.M., and J.W.S. designed research; Z.V., V.G., S.P., N.T., V.D., S.M., and J.W.S. performed research; Z.V., V.G., S.P., N.T., V.D., S.M., T.D., and J.W.S. analyzed data; and Z.V., S.M., T.D., G.H.M., and J.W.S. wrote the paper.

The authors declare no conflict of interest.

This article is a PNAS Direct Submission.

[1]To whom correspondence may be addressed. Email: jswan@mit.edu.

This article contains supporting information online at www.pnas.org/lookup/suppl/doi:10.1073/pnas.1901370116/-/DCSupplemental.

Published online June 4, 2019.

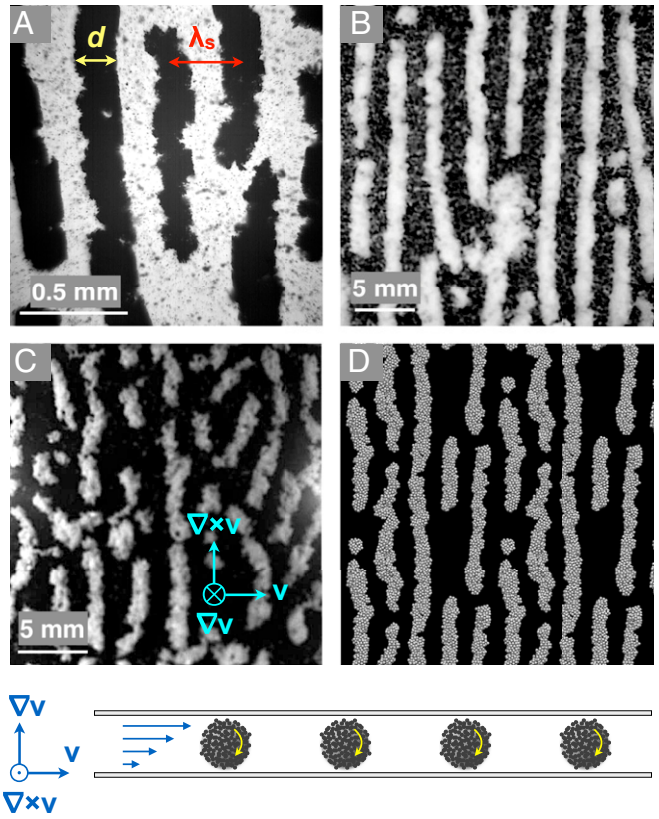

Fig. 1. Vorticity-aligned log-rolling structures obtained from experiments and simulations by shearing attractive particles in confined gaps. The horizontal direction corresponds to the velocity direction **v** and the vertical direction to the vorticity direction $\nabla \times \mathbf{v}$ so that the flow-gradient direction $\nabla \mathbf{v}$ is perpendicular to the pictures. The control parameters are [a, h, ϕ, $\dot{\gamma}$], where a is the mean particle radius, h the gap width of the shearing device, ϕ the volume fraction of the suspension, and $\dot{\gamma}$ the applied shear rate. (*A*) Dispersion of colloidal carbon black particles in mineral oil [135 nm, 173 μm, 1.5%, 0.9 s^{-1}]. The yellow and red arrows indicate the floc width d and the pattern wavelength λ_s, respectively. (*B*) Suspension of noncolloidal polyamide particles in water [9.4 μm, 1.5 mm, 5%, 0.8 s^{-1}]. (*C*) Suspension of noncolloidal hollow glass spheres in mineral oil bridged by water [6 μm, 1.5 mm, 3.1%, 20 s^{-1}]. (*D*) Dynamic simulation of sheared attractive particles with $h/a = 15$, $\phi = 16\%$, and Mason number $\mathrm{Mn} = 0.08$. See also additional pictures in *SI Appendix* and Movies S1–S11. The sketch below the images shows the geometry of the array of log-rolling flocs in the velocity–velocity gradient plane.

individual flocs (21, 22). However, clear experimental evidence for such an interpretation is lacking, and there is no detailed model that establishes a link between the floc viscoelastic properties and shear-induced structuring. Actually, no theory has yet been proposed to explain the physical mechanism responsible for the formation of these shear-induced patterns or to predict the wavelength or their stability.

To elucidate the mechanism underlying log formation in confined suspensions of attractive particles, we perform experiments on three different types of particles, both colloidal and noncolloidal, that we compare with discrete element simulations for volume fractions ϕ ranging from 0.01 to 0.2. Such simulations resolve the dynamics of individual particles among the aggregates. Of the many discrete element simulation methods, we have selected one that accurately treats the particle dynamics as overdamped and that takes into account the long-range hydrodynamic interactions mediated by the suspending fluid. Indeed, such interactions were shown to be crucial for recovering the flow-distorted microstructure observed in experiments on confined colloidal dispersions under shear (28) as well as the structural anisotropy associated with nonlinear rheology of colloidal gels (29). An important piece of previous work on attractive suspensions under shear was devoted to high packing fractions ($\phi > 0.4$) and used a simulation model in which only the lubrication forces between two neighboring particles were taken into account. In these simulations, particles were observed to form strings aligned in the flow direction and some more complex crystalline patterns, depending on the packing fraction and shear rate (30). None of these structures has been observed experimentally, and they do not correspond to the log-rolling flocs that we investigate here.

We show that shearing attractive particles in a confined geometry naturally leads to the formation of log-rolling flocs aligned along the vorticity direction through a purely hydrodynamic mechanism. Our dynamic simulations capture quantitatively the periodicity of the patterns and the size of the flocs observed experimentally using a variety of attractive particles. We argue that small fluctuations in the particle number density trigger hydrodynamic perturbations that lead to an array of corotating eddies in which particles aggregate to form the log-rolling flocs. This scenario is supported by an analysis of the simulated streamlines of the solvent flow. Finally, we provide measurements of the critical shear rate above which patterns do not form due to breakage of the aggregates by shear. This allows us to build a universal stability diagram for the log-rolling flocs in terms of a Mason number that measures the ratio of the shear force acting on particles to the interparticle attraction.

Results

Experiments. Our experimental observations of shear-induced pattern formation are summarized in Fig. 1 *A–C* for a variety of attractive suspensions sheared in confined geometries, namely (i) a colloidal gel of soot particles (carbon black) suspended in mineral oil and sheared under simple planar shear, (ii) a suspension of noncolloidal polyamide particles in water, and (iii) a capillary suspension of noncolloidal hollow glass spheres in mineral oil; both of the latter suspensions are sheared in a concentric cylinder (Taylor-Couette) cell. Attraction between the particles results, respectively, from (i) van der Waals interactions (31–34), (ii) "hydrophobic" forces (35, 36), and (iii) water capillary bridges (37, 38) (see *SI Appendix*, Table S1 and *Materials and Methods* for details). Going beyond previous reports on shear-induced structuring (21–26), Fig. 1 demonstrates that log-rolling flocs form perpendicular to the shearing direction whatever the origin of the attractive forces between the particles. Moreover, such a phenomenon is not restricted to colloidal dispersions since noncolloidal suspensions of particles up to 20 μm diameter display similar shear-induced patterns (Fig. 1 *B* and *C*). This prompts us to look for a universal mechanism mediated by hydrodynamic forces rather than by the nature of the interparticle forces or by the viscoelastic properties of the flocs. The discrete element simulations shown in Fig. 1*D* and detailed in the next paragraph exhibit a strikingly similar pattern of vorticity-aligned flocs.

Fig. 2 provides a full, quantitative characterization of the log-rolling floc patterns observed in the three experimental systems discussed above as well as in the simulations. For different gap spacings h, we systematically report the average floc width d and the average pattern wavelength λ_s in Fig. 2 *A* and *B*, respectively (*Materials and Methods*). When normalized by the mean particle radius a, all of the experimental data collapse remarkably onto master curves that span over two decades in the gap-to-particle size ratio h/a: We find that, up to experimental uncertainty, $d \approx h$ and $\lambda_s \approx 2.5h$. These results are robust to changes in the particle volume fraction ϕ, up to at least $\phi = 0.1$ (Fig. 2 *C* and *D*). To provide further insight into these experimental results, we turn to analysis of dynamical simulations.

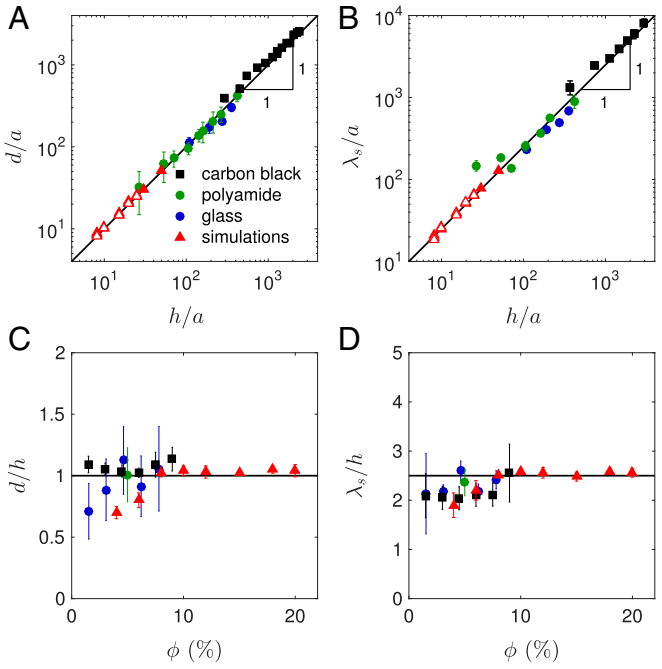

Fig. 2. Steady-state characteristics of the shear-induced patterns observed in experiments and in simulations. (*A* and *B*) Apparent diameter d of the vorticity-aligned flocs (*A*) and wavelength λ_s of the pattern normalized by the mean particle radius a and shown as a function of the gap width h normalized by a (*B*). (*C* and *D*) d/h (*C*) and λ_s/h (*D*) as a function of the volume fraction ϕ. Solid lines in *A*, *C* and *B*, *D* indicate $d = h$ and $\lambda_s = 2.5h$, respectively. Experiments are performed with carbon black particles (black squares), polyamide particles (green circles), and hollow glass spheres (blue circles). Simulations in *A* and *B* are performed at $\phi = 10\%$ (solid triangles) and $\phi = 15\%$ (open triangles).

Simulations. We perform discrete element simulations of noncolloidal particles. Athermal simulations yield faster computation and allow exploration of a greater parameter space while probing particle and flow geometries consistent with the experiments. The particles are suspended in a fluid of viscosity η and are subject to short-range attractive interactions. The suspension is confined by hard, parallel walls in a box of height h in the flow-gradient direction that is periodic in the flow-vorticity plane. The strain rate is set by the Mason number, $\mathrm{Mn} = 6\pi\eta a^2\dot{\gamma}/F$, which is the ratio of the shear forces exerted on a particle (by viscous shearing of the surrounding solvent) relative to the interparticle bond force at contact, F. The Rotne–Prager–Yamakawa (RPY) tensor (39) is used to account for the long-range hydrodynamic interactions among the particles and between the particles and the walls (see *Materials* and *Methods* for details).

Under all conditions explored, the suspension reaches a steady state under external shear after a strain $\gamma = \dot{\gamma}t \approx 100$. For a large range of Mason numbers, we observe strong vorticity alignment and the formation of log-rolling structures with a well-defined diameter and periodic spacing, very similar to that observed in the experiments (Fig. 1*D* and Movies S1–S11). We measure the average floc diameter d together with the wavelength λ_s of the pattern in steady state. Both quantities exhibit the same scaling with the gap size h as observed in the experiments (Fig. 2 *A* and *B*). The floc width and the pattern spacing are also independent of the particle volume fraction, ϕ, as in the experiments. Simulations allow us to explore a range of volume fractions up to 20% (Fig. 2 *C* and *D*). These results confirm that fixing the ratio of wall gap to particle size while increasing ϕ leads to flocs with a denser internal structure.

The simulations also reveal that there is a critical initial packing fraction $\phi_{\max} \simeq 0.2$ beyond which the suspension is too dense to separate into stable logs. We estimate $\phi_{\max}$ using conservation of the total number of particles. The particles initially occupy a volume $L_x L_y h$, where L_x and L_y stand for the box dimensions in the flow-vorticity plane, before being redistributed into N logs of diameter d and interlog space of λ_s. The maximum packing fraction that can be reached inside a log corresponds to random close packing; e.g., for spheres, $\phi_{\mathrm{rcp}} \approx 0.63$. The conservation of the number of particles expressed per unit length along the vorticity direction reads $\phi_{\mathrm{rcp}} N\pi(d/2)^2 = \phi_{\max} L_x h$, where $N = L_x/\lambda_s$ is the number of logs in the flow domain. Therefore the maximum volume fraction admitting a periodic array of logs is $\phi_{\mathrm{rcp}}(\pi d^2)/(4\lambda_s h)$, which is about 0.2 when $d = h$ and $\lambda_s = 2.5h$.

Although the total computational time for the simulations becomes prohibitive for large systems, the simulations probe suspensions and geometries that are only slightly more confined ($h/a = 8$–50) than in experiments ($h/a = 25$–$2{,}500$). Where the range of confinement overlaps between the experiments and the simulations, good correspondence in the properties of the flocs is observed. Fig. 2 validates the use of discrete element simulations with long-range hydrodynamic interactions to model the steady-state properties of the vorticity-aligned flocs. Using this same modeling approach, we explore the mechanism responsible for shear-induced pattern formation.

Discussion

Wavelength Selection Mechanism. Consider first the case of force- and torque-free solid cylinders immersed in a shear flow perpendicular to their axis and centered between counter-translating parallel walls. By symmetry, any periodic cylinder pattern with intercylinder spacing, λ_s, is stable and such a configuration would be persistent in time (42). Therefore, a periodic array of solid cylinders has no wavelength selection mechanism. On the contrary, the logs observed experimentally are not solid but porous and built from shear-induced aggregates of freely suspended attractive particles. Given these considerations, we treat a single aggregate as a rotating body between two stationary parallel plates as depicted in Fig. 3. When the aggregate is infinite in extent, the induced flow fields to the left and right of the aggregate resemble that in a lid-driven cavity, for which the cavity is very deep (43). It was first shown by Moffatt (40) that such a configuration should generate an infinite set of counter-rotating eddies all of the same size and spaced periodically. If a simple shear flow with shear rate equal to the rate of rotation of the aggregate is superimposed onto this flow field, the symmetry is broken and the eddies that counter rotate with aggregate are canceled out and the corotating eddies are enhanced (41). This superposition of the flow due to a rotating cylinder and a simple shear between parallel walls leads to a periodic array of corotating eddies spaced by $\lambda_s \simeq 2.78h$, very close to the spacing between logs measured in experiments. Moffatt's set of eddies is driven not by a solid cylinder, but by a line torque oriented along the vorticity direction of the imposed shear flow. In the near field such a superposition fails to satisfy a no-slip condition of the surface of the aggregate. However, in the far field (on distances farther than the channel spacing) hydrodynamic screening ensures that Moffatt's flow field dominates. This makes it the appropriate analytical base flow for understanding coordination among vorticity-aligned aggregates.

This scenario suggests the following process occurs during shear-induced structure formation. The imposed shear flow disrupts an initially homogeneous suspension microstructure, leading to the formation of aggregates. These aggregates play the role of local, rotlet-like (point torque) disturbances generating a series of eddies separated by stagnation points. Free-floating

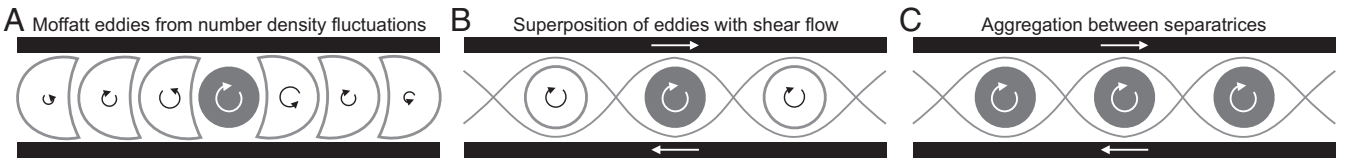

Fig. 3. The hydrodynamic mechanism responsible for the log-rolling phenomenon. (*A*) The flow field around a randomly formed particle aggregate or log (dark gray) resembles a lid-driven cavity in which the cavity is very deep. Therefore, it contains a roughly periodically spaced set of counter-rotating separatrices (cells with arrows) moving along the channel with periodic spacing (40). (*B*) If this perturbation flow field is superimposed with simple shear flow at the upper and lower boundaries, the shear flow cancels out cells that counter rotate and enhances the corotating separatrices that have a stable spacing of $\lambda_s \sim 2.78h$ (41). (*C*) In an attractive suspension, the centers of the eddies act as stable stagnation points for the particle flow, where particles further aggregate into logs.

particles and small aggregates are driven away from the separatrices to concentrate within the eddies and eventually grow to form stable logs. These vorticity-aligned flocs maintain their separation due to the hydrodynamic forces induced by the shear flow between the parallel walls. Within this hydrodynamic framework, free particles in solution may generate fluctuations that can cause partially formed logs to oscillate back and forth between adjacent eddies (see Movies S6 and S7 for simulations and Movie S5 for similar effects in experiments). Prior work on inertial pipe flows has used a similar analysis of streamlines in the frame moving with the mean flow to explain alignment of particles in suspension. In this scenario, a recirculating flow at finite Reynolds number leads to stagnation points that align particles in trains along the flow direction (44). When an aggregate that does not span the entire vorticity direction already occupies one of the eddies, defects may arise as other logs will bend to occupy two stable locations along their length, as evidenced in *SI Appendix*, Figs. S1, *ii*; S2, *iii*; and S3*D*. These bends are observed only in periodic arrays of vorticity-aligned flocs and can be thought of as defects in a crystal of flocs that are sustained by the same hydrodynamic forces (45).

Approach to Stable Spacing. If the separatrices located between rotating eddies are indeed responsible for the pattern formation, then a sheared dispersion under confinement should naturally evolve toward the periodic spacing that the log-rolling structures exhibit in steady state. To examine this, we perform a set of simulations where the initial particle number density along the flow direction is periodically modulated. An initial periodic number density profile is imposed with a wavelength λ_0 along the flow direction and fixed total particle volume fraction ϕ_0: $\phi(x, \gamma = 0) = \phi_0[1 + \sin(2\pi x/\lambda_0)]$. We vary λ_0 relative to the stable wavelength λ_s and track the evolution of the instantaneous characteristic spacing in the pattern, $\lambda(\gamma)$, as a function of the accumulated strain γ. Irrespective of λ_0, the system evolves toward the stable periodic spacing observed experimentally and in the previously unseeded simulations (Fig. 4*A*). There does not appear to be a competing stable steady state for the sheared dispersion, which provides strong support for the proposed hydrodynamic scenario.

The exact path of the dynamical system to steady state does, however, strongly depend on λ_0 and more specifically on whether the imposed density fluctuations have a wavelength smaller or larger than λ_s. For $\lambda_0 > \lambda_s$ the dominant instantaneous wavelength steadily decreases toward the stable state, λ_s, and displays a power-law decay $(\lambda - \lambda_s) \sim \gamma^{-0.67}$ (Fig. 4*B*). As shown in Fig. 4*D* for $\lambda_0 = 4\lambda_s$, the initially broad distribution of particles (at $\gamma = 1$) separates early on into several particle-rich regions (at $\gamma = 5$–40) until the particles are eventually aggregated into logs with the stable spacing $\lambda_s = 2.5h$. In contrast, for $\lambda_0 < \lambda_s$, $\lambda(\gamma)$ exhibits a maximum as the length of the periodic box transiently becomes the dominant wavelength and no algebraic decay with strain is observed (Fig. 4*C*). As seen in Fig. 4*E*, when starting with a shorter seeded wavelength, the initial straining leads to a more homogeneous, uniform state ($\gamma = 5$–20). In this uniform dispersion, similar to the randomly distributed initial configurations discussed above, local fluctuations lead to the growth of density variations in the flow direction and the characteristic spacing gradually develops with accumulating strain ($\gamma = 40$–100).

As the simulations account for the hydrodynamics implicitly through the interparticle hydrodynamic interactions, we introduce a few tracer particles in our simulations to probe the fluid streamlines. Such tracers do not interact with other

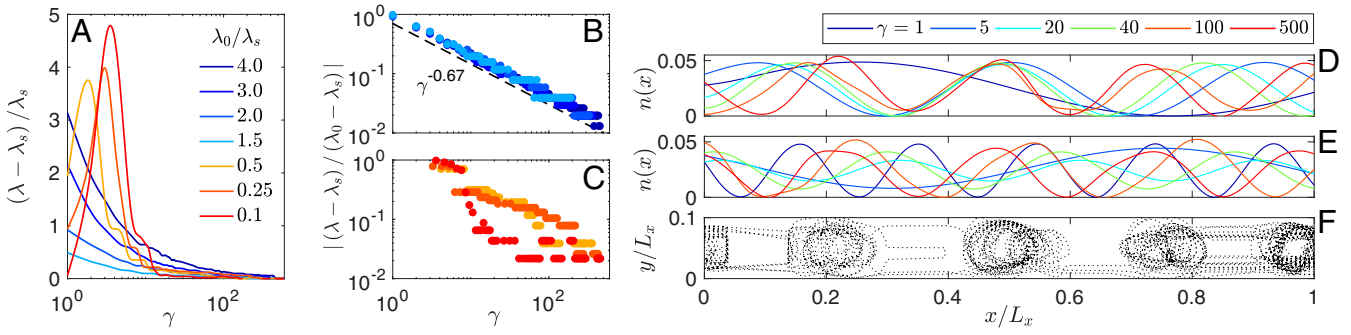

Fig. 4. Simulations confirm that there exists only one single stable wavelength for the log-rolling pattern, $\lambda_s = 2.5h$. (*A*) The evolution of the pattern wavelength λ with strain γ toward steady state after imposing an initial particle number density distribution in the flow direction with wavelength λ_0 for an overall volume fraction $\phi_0 = 0.15$ and gap width $h = 10a$. The details of the dynamical approach to λ_s strongly depend on λ_0. (*B*) For $\lambda_0 > \lambda_s$, the absolute distance to λ_s normalized on the initial distance, $\lambda_0 - \lambda_s$ decays as a power law with an exponent of about $-2/3$. (*C*) For $\lambda_0 < \lambda_s$, the dynamics do not display a continuous algebraic decay. (*D* and *E*) The local particle number density distribution $n(x)$ in the (**v**, ∇**v**) plane plotted for increasing total strain γ for (*D*) $\lambda_0/\lambda_s = 4$ and (*E*) $\lambda_0/\lambda_s = 1/4$. In the second case, the distribution first becomes increasingly uniform at intermediate strains ($\gamma = 5$–20) and the final pattern emerges only for $\gamma > 100$. (*F*) Trajectories of noninteracting tracer particles in simulations with $\lambda_0/\lambda_s = 4.0$ for $\gamma > 100$.

particles and passively follow the fluid flow. As shown in Fig. 4*F*, the tracer motion is mostly localized, corotating around in the eddies with occasional exchanges between neighboring eddies. We observe that the tracers concentrate at the exact same positions as the peaks in the final particle number density distribution $n(x)$, supporting the hydrodynamic mechanism for log formation and propagation. This confirms our hypothesis that the shear-induced patterns observed experimentally indeed arise due to the well-known hydrodynamics of the lid-driven cavities.

Stability Diagram for Pattern Formation. In the experiments, as well as in the simulations, the steady-state features of the pattern are independent of the imposed shear rate over a large range of values. However, when a strong shear rate is applied above a critical value $\dot{\gamma}_c$, log-rolling flocs do not form and the suspension remains fully dispersed (Fig. 5, *Inset*). Direct comparison between the transitions observed in experiments and simulations is made on the basis of a critical Mason number Mn_c. Fig. 5 shows that all experimental data collapse onto a single master curve Mn_c vs. h/a that nicely extends the stability boundary of the simulations, provided an appropriate interparticle force F is used to define the Mason number for the various suspensions (see *SI Appendix*, Table S1 for the parameters used in Fig. 5).

As detailed in *SI Appendix*, the order of magnitude found for F is reasonable for all experimental systems and even supported quantitatively by direct force measurements through atomic force microscopy in the case of polyamide particles. Thus, the stability boundary is independent of the type of dispersion and can be described by a power-law behavior, $\mathrm{Mn}_c \sim (h/a)^{-1.4}$, over almost three orders of magnitude in the gap-to-particle size ratio. Such a scaling can be understood in terms of a simple force balance between the viscous drag force acting on an aggregate and the attractive interparticle forces that keep individual particles together. In the process of forming the logs, aggregates of characteristic size h must form. The stresslet exerted on such a floc scales as $\eta\dot{\gamma}h^3$. Such a stresslet can break a floc by severing the interparticle bonds in the plane of shear. For a floc having fractal dimension d_f, the shear strength scales with the number of bonds in the shear plane, $\sim h^{d_f-1}$, and with the attractive force between the particles. The stresslet balances the shear strength at the critical Mason number so that $\mathrm{Mn}_c \sim h^{d_f-4}$. Using the scaling exponent of -1.4 observed in both experiments and simulations, we infer a fractal dimension of the flocs, $d_f = 2.6$, which is consistent with the fractal dimension expected for shear-induced flocculation (46).

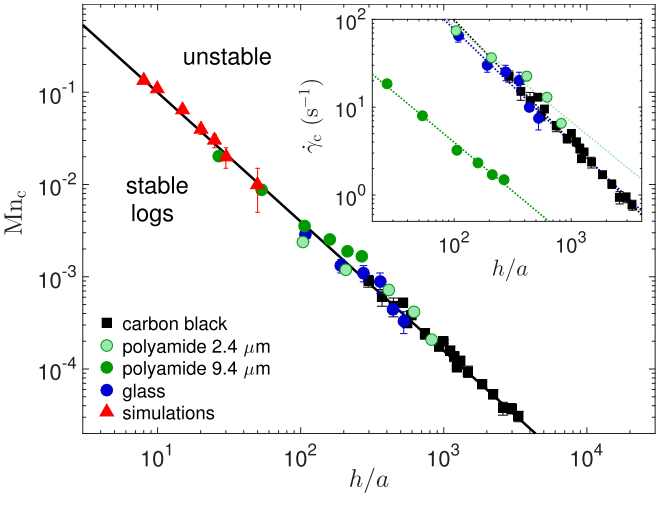

Fig. 5. Stability diagram for shear-induced patterns: critical Mason number Mn_c above which log-rolling flocs are unstable as a function of the gap width h normalized by the mean particle radius a. The solid line is $\mathrm{Mn}_c = 2.5\,(h/a)^{-1.4}$. Shown are the same symbols as in Fig. 1. Light green (dark green resp.) circles refer to polyamide particles with $a = 2.4$ μm ($a = 9.4$ μm resp.). *Inset* shows the raw experimental data together with their best power-law fits in terms of the critical shear rate $\dot{\gamma}_c$ above which log-rolling flocs do not form. In the main graph, experimental Mason numbers were scaled to collapse the data on a single master curve. All fitting and scaling parameters are gathered in *SI Appendix*, Table S1.

Conclusion

Pattern formation in suspensions of attractive particles confined and sheared between parallel plates results from hydrodynamic coupling between the particle-rich flocs and the confining boundaries. The flow field generated by a local particle number density fluctuation coupled to the externally applied shear flow generates a succession of corotating eddies. Separatrices between the eddies cause particles to accumulate within each eddy, producing a periodic array of log-rolling flocs. The mechanism is insensitive to particle-level details, which explains why shear-induced structuring is observed for a wide range of both colloidal and noncolloidal attractive particles. The stability of the log-rolling states is given by a balance between viscous drag on the fractal aggregates and the cohesive force due to interparticle attraction. The scaling relations derived from the experimental, theoretical, and computational results in this work open the way for better control of the structure of attractive suspensions under confined shear and the possibility of using flow fields for assembly of dispersed microscale particles into macroscale patterns with long-range order.

Materials and Methods

Experiments. Four different suspensions are used in the present study (*SI Appendix*, Table S1). In addition, three different shearing setups are involved in imaging the suspensions. Carbon black gels are sheared in a homemade plane-shear cell consisting of two parallel glass plates separated by a constant gap and in a rheo-optical setup consisting of a parallel-plate geometry attached to a stress-controlled rheometer (Anton-Paar; MCR 301). Shear-induced structuring in noncolloidal suspensions of polyamide particles and of hollow glass spheres is achieved in concentric-cylinder (or Taylor-Couette) shear cells, the inner cylinder being connected to a stress-controlled rheometer (TA Instruments; AR1000 and ARG2). Pictures and movies of the sheared suspensions are taken with standard CCD cameras. Electron microscopy images of the polyamide particles were recorded by a scanning electron microscope (SEM) (Zeiss Supra 55VP). We also used an atomic force microscope (AFM) (JPK Nanowizard 4) to estimate the attractive force between polyamide particles. Full experimental details are given in *SI Appendix*.

Simulations. The positively split Ewald (PSE) (47, 48) is used for discrete element simulations of spherical particles with low Reynolds number hydrodynamic interactions accounted for by the RPY approximation. Particles in suspension have a mean radius a and an imposed polydispersity of $\sigma = 5\%$. The short-ranged interparticle attraction is modeled with an Asakura–Oosawa form (49) of width $\delta/a = 0.2$ and depth U. We focus on athermal systems and therefore set the thermal energy scale to $k_BT = 0$. The strength of shear is varied by adjusting the strain rate $\dot{\gamma}$ and the dispersion is strained for $\gamma = 600$ strain units. The Mason number $\mathrm{Mn} = 6\pi\eta a^2\dot{\gamma}\delta/U$ characterizes the ratio of the shear force exerted on the particles to the attractive interparticle force. In these simulations, hydrodynamic lubrication is neglected for computational expediency. However, recent work has shown that in dispersions of rigid particulate aggregates, for which relative motion between nearly touching particles is minimal, hydrodynamic lubrication has only a marginal effect on the structure and dynamics (29, 50). Confining walls are represented by a hexagonal close-packed lattice of spherical particles connected to each other through rigid, harmonic bonds. The walls interact hydrodynamically with particles of the colloidal dispersion and exert a hard repulsion at contact (51).

ACKNOWLEDGMENTS. We gratefully acknowledge the financial support from the Massachusetts Institute of Technology-France seed fund, the CNRS via the Projet International de Coopération Scientifique-USA scheme (36939), and the Technology Initiative's France program. This research was

supported in part by the National Science Foundation (NSF) under Grants NSF PHY 17-48958 and CBET 15-54398. We thank Bavand Keshavarz for machining the cylindrical bobs used with suspensions of polyamide particles. N.T, V.D., and S.M. thank Catherine Barentin, Etienne Barthel, and Denis Bartolo for fruitful discussions as well as Joseph Pierre and Agnès Piednoir for technical help with atomic force microscopy.

1. R. Zenit, J. J. Feng, Hydrodynamic interactions among bubbles, drops, and particles in non-Newtonian liquids. *Annu. Rev. Fluid Mech.* **50**, 505–534 (2018).
2. A. Einstein, Eine neue Bestimmung der Moleküldimensionen. *Annalen der Physik* **324**, 289–306 (1906).
3. A. Einstein, Berichtigung zu meiner Arbeit: Eine neue Bestimmung der Moleküldimensionen. *Annalen der Physik* **339**, 591–592 (1911).
4. M. Maxey, Simulation methods for particulate flows and concentrated suspensions. *Annu. Rev. Fluid Mech.* **49**, 171–193 (2017).
5. M. Duduta *et al.*, Semi-solid lithium rechargeable flow battery. *Adv Energy Mater* **1**, 511–516 (2011).
6. H. Parant *et al.*, Flowing suspensions of carbon black with high electronic conductivity for flow applications: Comparison between carbons black and exhibition of specific aggregation of carbon particles. *Carbon* **119**, 10–20 (2017).
7. D. B. Genovese, J. E. Lozano, M. A. Rao, The rheology of colloidal and noncolloidal food dispersions. *J. Food Sci.* **72**, R11–R20 (2007).
8. M. C. Marchetti *et al.*, Hydrodynamics of soft active matter. *Rev. Mod. Phys.* **85**, 1143–1189 (2013).
9. S. C. Takatori, J. F. Brady, Superfluid behavior of active suspensions from diffusive stretching. *Phys. Rev. Lett.* **118**, 018003 (2017).
10. J. Stickel, R. Powell, Fluid mechanics and rheology of dense suspensions. *Annu. Rev. Fluid Mech.* **37**, 129–149 (2005).
11. V. Michailidou, G. Petekidis, J. Swan, J. Brady (2009), Dynamics of concentrated hard-sphere colloids near a wall. *Phys. Rev. Lett.* **102**, 068302 (2009).
12. F. Boyer, E. Guazzelli, O. Pouliquen, Unifying suspension and granular rheology. *Phys. Rev. Lett.* **107**, 188301 (2011).
13. X. Cheng, X. Xu, S. A. Rice, A. R. Dinner, I. Cohen, Assembly of vorticity-aligned hard-sphere colloidal strings in a simple shear flow. *Proc. Natl. Acad. Sci. U.S.A.* **109**, 63–67 (2012).
14. R. Wessel, R. C. Ball, Fractal aggregates and gels in shear flow. *Phys. Rev. A* **46**, 3008–3011 (1992).
15. M. Cloitre, R. T. Bonnecaze, A review on wall slip in high solid dispersions. *Rheol. Acta* **56**, 283–305 (2017).
16. P. Chaudhuri, L. Berthier, L. Bocquet, Inhomogeneous shear flows in soft jammed materials with tunable attractive forces. *Phys. Rev. E* **85**, 021503 (2012).
17. E. Irani, P. Chaudhuri, C. Heussinger, Impact of attractive interactions on the rheology of dense athermal particles. *Phys. Rev. Lett.* **112**, 188303 (2014).
18. T. Divoux, M. A. Fardin, S. Manneville, S. Lerouge, Shear banding of complex fluids. *Annu. Rev. Fluid Mech.* **48**, 81–103 (2016).
19. D. Bonn, M. M. Denn, L. Berthier, T. Divoux, S. Manneville, Yield stress materials in soft condensed matter. *Rev. Mod. Phys.* **89**, 035005 (2017).
20. J. J. V. DeGroot, C. W. Macosko, T. Kume, T. Hashimoto, Flow-induced anisotropic SALS in silica-filled PDMS liquids. *J. Colloid Interf. Sci.* **166**, 404–413 (1994).
21. A. Montesi, A. Peña, M. Pasquali, Vorticity alignment and negative normal stresses in sheared attractive emulsions. *Phys. Rev. Lett.* **92**, 058303 (2004).
22. S. Lin-Gibson, J. A. Pathak, E. A. Grulke, H. Wang, E. K. Hobbie, Elastic flow instability in nanotube suspensions. *Phys. Rev. Lett.* **92**, 048302 (2004).
23. C. O. Osuji, D. A. Weitz, Highly anisotropic vorticity aligned structures in a shear thickening attractive colloidal system. *Soft Matter* **4**, 1388–1392 (2008).
24. V. Grenard, N. Taberlet, S. Manneville, Shear-induced structuration of confined carbon black gels: Steady-state features of vorticity-aligned flocs. *Soft Matter* **7**, 3920–3928 (2011).
25. A. Negi, C. Osuji, New insights on fumed colloidal rheology–shear thickening and vorticity-aligned structures in flocculating dispersions. *Rheol. Acta* **48**, 871–881 (2009).
26. A. Karppinen *et al.*, Flocculation of microfibrillated cellulose in shear flow. *Cellulose* **19**, 1807–1809 (2012).
27. M. P. Godfrin *et al.*, Shear-directed assembly of graphene oxide in aqueous dispersions into ordered arrays. *Langmuir* **29**, 13162–13167 (2013).
28. D. R. Foss, J. F. Brady, Structure, diffusion and rheology of Brownian suspensions by Stokesian dynamics simulation. *J. Fluid Mech.* **407**, 167–700 (2000).
29. Z. Varga, J. W. Swan, Large scale anisotropies in sheared colloidal gels. *J. Rheol.* **62**, 405–418 (2018).
30. L. E. Silbert, J. R. Melrose, R. C. Ball, The rheology and microstructure of concentrated, aggregated colloids. *J. Rheol.* **43**, 673–700 (1999).
31. M. van der Waarden, Stabilization of carbon black dispersion in hydrocarbons. *J. Colloid Sci.* **5**, 317–325 (1950).
32. P. Hartley, G. Parfitt, Dispersion of powders in liquids. 1. The contribution of the van der Waals force to the cohesiveness of carbon black powders. *Langmuir* **1**, 651–657 (1985).
33. V. Trappe *et al.*, Investigation of q-dependent dynamical heterogeneity in a colloidal gel by x-ray photon correlation spectroscopy. *Phys. Rev. E* **76**, 051404 (2007).
34. J. J. Richards, J. B. Hipp, J. K. Riley, N. J. Wagner, P. D. Butler, Clustering and percolation in suspensions of carbon black. *Langmuir* **33**, 12260–12266 (2017).
35. E. E. Meyer, K. J. Rosenberg, J. Israelachvili, Recent progress in understanding hydrophobic interactions. *Proc. Natl. Acad. Sci. U.S.A.* **103**, 15739–15746 (2006).
36. J. N. Israelachvili, *Intermolecular and Surface Forces* (Academic Press, 2011).
37. E. Koos, N. Willenbacher, Capillary forces in suspension rheology. *Science* **331**, 897–900 (2011).
38. E. Koos, Capillary suspensions: Particle networks formed through the capillary force. *Curr. Opin. Colloid Interf. Sci.* **19**, 575–584 (2014).
39. J. Rotne, S. Prager, Variational treatment of hydrodynamic interaction in polymers. *J. Chem. Phys.* **50**, 4831–4837 (1969).
40. H. K. Moffatt, Viscous and resistive eddies near a sharp corner. *J. Fluid Mech.* **18**, 1–18 (1964).
41. M. Wilson, P. Gaskell, M. Savage, Nested separatrices in simple shear flows: The effect of localized disturbances on stagnation lines. *Phys. Fluids* **17**, 093601 (2005).
42. S. Kim, S. J. Karrila, *Microhydrodynamics: Principles and Selected Applications* (Courier Corporation, 2013).
43. M. Hellou, M. Coutanceau, Cellular Stokes flow induced by rotation of a cylinder in a closed channel. *J. Fluid Mech.* **236**, 557–577 (1992).
44. J. P. Matas, V. Glezer, E. Guazzelli, J. F. Morris, Trains of particles in finite-Reynolds-number pipe flow. *Phys. Fluids* **16**, 4192–4195 (2004).
45. J. W. Swan, J. F. Brady, Particle motion between parallel walls: Hydrodynamics and simulation. *Phys. Fluids* **22**, 103301 (2010).
46. V. Oles, Shear-induced aggregation and breakup of polystyrene latex particles. *J. Colloid Interf. Sci.* **154**, 351–358 (1992).
47. A. M. Fiore, F. Balboa Usabiaga, A. Donev, J. W. Swan, Rapid sampling of stochastic displacements in Brownian dynamics simulations. *J. Chem. Phys.* **146**, 124116 (2017).
48. A. M. Fiore, J. W. Swan, Rapid sampling of stochastic displacements in Brownian dynamics simulations with stresslet constraints. *J. Chem. Phys.* **148**, 044114 (2018).
49. S. Asakura, F. Oosawa, Interaction between particles suspended in solutions of macromolecules. *J. Polym. Sci. A Polym. Chem.* **33**, 183–192 (1958).
50. Z. Varga, J. W. Swan, Normal modes of weak colloidal gels. *Phys. Rev. E* **97**, 012608 (2018).
51. J. W. Swan, J. F. Brady, Simulation of hydrodynamically interacting particles near a no-slip boundary. *Phys. Fluids* **19**, 113306 (2007).